

## Research

# Prediction of thermal cycling behaviour of Ni-rich NiTi SMA using empirical and artificial neural network modelling

Swaminathan Ganesan<sup>1</sup> · Shreyash Pandey<sup>2</sup> · Senthilkumar Krishnasamy<sup>1</sup> · Senthil Muthu Kumar Thiagmani<sup>3</sup>

Received: 6 November 2024 / Accepted: 3 February 2025

Published online: 23 February 2025

© The Author(s) 2025 [OPEN](#)

## Abstract

NiTi SMAs, also known as Nitinol, are well-known and widely used due to their unique properties. This study predicts the transformation behaviour of a binary near-equiatomic shape memory alloy (SMA) during thermal cycling using empirical and ANN-based models. The input data was generated through thermal cycling tests using a differential scanning calorimeter (DSC) under a nitrogen atmosphere, wherein the maximum and minimum temperatures were varied based on the transformation temperatures of the alloy. Three different models, i.e. symmetrical, asymmetrical and artificial neural network (ANN), were developed to understand the transformation behaviour of the alloy using the same set of test data for validation. For qualitative and quantitative comparisons of the model, priority was given to the simplicity of the model (minimum variables) and the accuracy of the prediction. The results show that the ANN-based model can predict the transformation behaviour more accurately (99.81%) as compared to the conventional empirical models, i.e., symmetric (96.64%) and asymmetric models (98.14%).

**Keywords** NiTi SMA · Thermal cycling · Transformation temperatures · Gaussian model · Artificial neural network

## 1 Introduction

Shape memory alloys are a class of smart materials that have proven to be the most successful materials for engineering and medical applications due to their ability to exhibit two distinct properties: the superelastic effect and the shape memory effect [1]. In the superelastic effect, after undergoing deformation under significant strain (~8%) by loading and unloading, they recover their original shape [2]. In the shape memory effect, they can revert to their original undeformed state when provided the stimulus at the stable deformed configuration. This process happens in two distinct phases: parent phase, i.e., austenite (A) and product phase, i.e., martensite (M) [3]. Generally, austenite is a high-temperature phase exhibiting higher crystal symmetry, and martensite is a low-temperature phase exhibiting lower crystal symmetry than austenite. In NiTi-based alloys, the crystal structure of the austenitic phase is B2 (cubic), and the martensitic phase is B19' (monoclinic) [4, 5].

The mechanism of SME is based on microstructural changes caused by the phase transformations occurring between A and M. When SMA is deformed in its martensitic phase (low-temperature phase) followed by heating it, transformation to the austenitic phase (high-temperature phase) takes place. During this transformation, the alloy regains its original

---

✉ Swaminathan Ganesan, swaminathan@psgitech.ac.in | <sup>1</sup>Department of Mechanical Engineering, PSG Institute of Technology and Applied Research, Coimbatore, Tamil Nadu 641062, India. <sup>2</sup>Department of Metallurgy and Materials Engineering, Indian Institute of Engineering Science and Technology, Shibpur, West Bengal 711103, India. <sup>3</sup>Department of Mechanical Engineering, Kalasalingam Academy of Research and Education, Krishnankoil, Tamil Nadu 626126, India.



shape with negligible residual strain [6]. Upon further cooling back to martensite, two possibilities are there, i.e., either it remains undeformed after cooling (one-way SME), or it transforms back to the deformed shape (two-way SME) [7, 8]. Throughout these transformations, four critical temperatures are defined, namely martensite start temperature ( $M_s$ ), martensite finish temperature ( $M_f$ ), austenite start temperature ( $A_s$ ) and austenite finish temperature ( $A_f$ ), as shown in Fig. 1 [9–11].

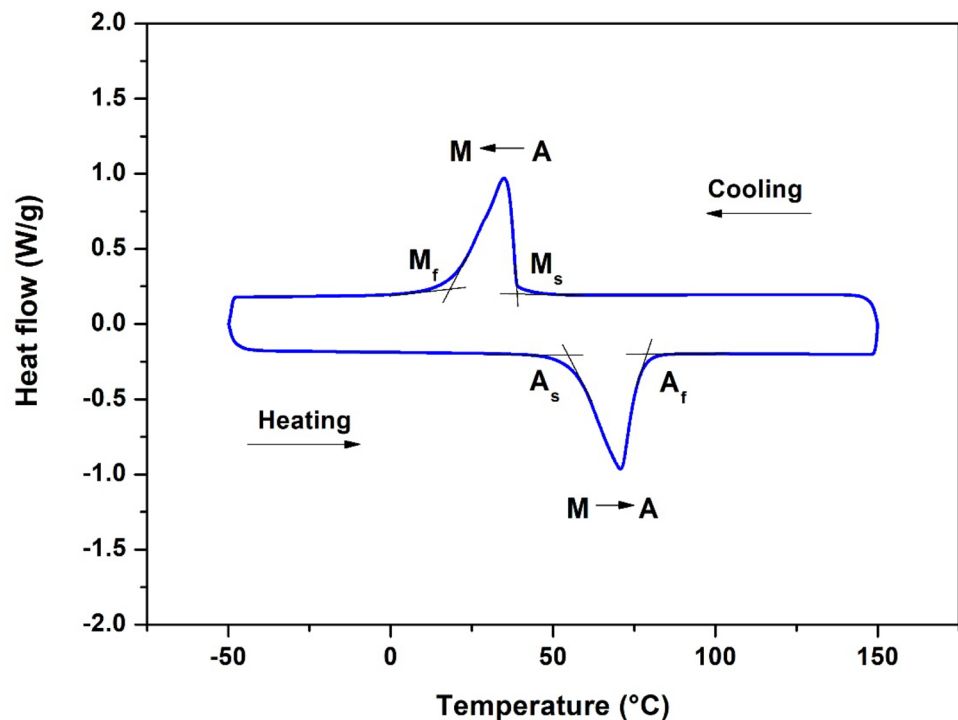
The shape memory effect was first observed in an Au-Cd alloy, following which many systems (NiTi, Cu-, Fe-based) have been found to exhibit shape memory properties over the years [12]. Ni-Ti alloys (Nitinol) are among the most critical alloy systems because of their unique properties, such as SME, biocompatibility, high corrosion resistance, and high strength-to-weight ratio [13, 14]. Nitinol was discovered in 1962 by J Buehler and his team at the Naval Ordnance Laboratory, USA [15, 16]. NiTi alloys have found applications across different fields of science and technology, including biomedical devices, dental equipment, aerospace and automotive components and robotic arms [10, 17]. Many of the applications for SMAs are based on SMEs, i.e., heating and cooling (repeatedly or occasionally), to trigger the phase transformation and shape change [18].

The prolonged use of SMAs in many applications may cause deterioration of functional properties of the alloys, and this degradation in functional properties, such as  $M_s$ ,  $M_f$ ,  $A_s$ ,  $A_f$ , recovery stress, recovery strain, stress hysteresis and thermal hysteresis, is called functional fatigue [19, 20]. This results from repeated cyclic phase transformations because several microstructural changes, such as the generation of crystal defects (dislocations) and the retention of retained martensite, occur [21]. SMA cycling is classified into thermal and thermomechanical cycling. Thermal cycling is a stress-free heating and cooling cycle, whereas thermomechanical cycling involves a heating and cooling cycle under constant stress [22].

Controlling the conditions during thermal cycling carefully minimizes functional fatigue and aging effects [23, 24]. In order to address these problems and make Nitinol more stable during thermal cycling, appropriate material selection, design considerations, and optimization of processing parameters are essential. This poses a need for computational modelling to design and optimize the operating parameters. Computational modelling has increased research efficiency due to its cost-effectiveness and time-efficient approach to studying and addressing the challenges associated with various aspects of materials.

It enables the exploration of material behaviour prediction and optimization of operating parameters, thereby contributing to improved reliability and performance [25, 26]. In this study, the Gaussian symmetrical and asymmetrical double sigmoidal models were used because they converge more accurately with the experimental data than the other models, which are too complex or do not converge well. The ANN model was also developed to predict the behaviour more accurately than the empirical models. The primary objective of this work is to develop and study empirical models

**Fig. 1** DSC thermogram illustrating the transformation temperatures of a typical shape memory alloy (NiTi SMA) during heating and cooling



to predict the transformation behaviour of Nitinol during thermal cycling. This study has developed two empirical models, i.e., Gaussian-based symmetrical and asymmetrical models, and an ANN-based model. All the models are developed using the same thermal cycling dataset.

## 2 Methodology

### 2.1 Experimental methodology

Ni<sub>50.7</sub>Ti<sub>49.3</sub> (at.%) alloy sheet with a thickness of 0.5 mm was used in this study. This sheet was initially solutionized at 900 °C for 3.6 ks, followed by water quenching at room temperature. Sheets with 3.5 × 3.5 mm<sup>2</sup> dimensions were machined using a wire-cut electro-discharge machine from the solutionized sheet. These sheets were used as test specimens to conduct thermal cycling studies using a differential scanning calorimeter (Discovery DSC 25, made by TA Instruments) under the nitrogen atmosphere. The transition temperatures were determined by applying the tangent line method, as shown in Fig. 1. During thermal cycling, the alloys were repeatedly subjected to heating and cooling at a rate of 20 °C/min within the temperature range of – 50 to 150 °C for 15 cycles (until the changes in the transformation temperatures are saturated). This is based on the transformation temperatures of the alloy chosen, i.e., binary NiTi SMA. All four transformation temperatures, i.e., A<sub>s</sub>, A<sub>f</sub>, M<sub>s</sub> and M<sub>f</sub>, lie within this range, as shown in Fig. 1. More details about the experiment can be found elsewhere [27].

### 2.2 Empirical model

It can be clearly observed from Fig. 1 that both A → M and M → A transformation curves are asymmetrical. However, initially, the Gaussian (symmetrical model) was chosen to understand the transformation behaviour because of its simplicity and preciseness compared with other models [28–30]. After the Gaussian curve was finalised for the model, the terms in the Gaussian equation were modified to fit the shape memory characteristics, as shown in Eq. 1.

$$H = H_0 + \left( \frac{A}{w \times \sqrt{\pi/2}} \right) \times e^{-2(T-T_c)/w^2} \quad (1)$$

where, H = Heat flow, H<sub>0</sub> = Initial heat flow (heat flow in the first cycle), T = Temperature, A, T<sub>c</sub>, and w are curve-shaping factors.

Characteristics of all these equation parameters were analysed. For simplification, the heating and cooling curves were separately analysed. It was done to optimise the empirical model by using distinct values of equation parameters for heating and cooling curves. Each parameter was individually analysed to determine the behaviour of 'A', 'w', and 'T<sub>c</sub>' during thermal cycling. The parameter analysis mainly focused on the variation in shape memory characteristics with increasing cycles (n).

After successfully developing a symmetrical model and a basic understanding of the parameters, an attempt was made to improve its accuracy. The introduction of asymmetry in the model was necessary. Hence, the Double sigmoidal model was chosen after the rigorous analysis of various standard asymmetrical peak functions to achieve higher accuracy [31, 32]. The equation of the Double sigmoidal model, shown in Eq. 2, was analysed like the Gaussian model.

$$H = H_0 + \left( \frac{A}{1 + e^{-\left(\frac{T-T_c + \frac{w1}{2}}{w2}\right)}} \right) \times \left( 1 - \frac{1}{1 + e^{-(T-T_c - w1/2)/w3}} \right) \quad (2)$$

where, H = Heat Flow, H<sub>0</sub> = Initial heat flow (heat flow in the first cycle), A, T<sub>c</sub>, w1, w2, and w3 are curve-shaping factors.

Apart from A and T<sub>c</sub>, there are three w(s), i.e., w1, w2 and w3. The 'w' factor alters the shape of the peak curve. These three w(s) bring the asymmetry, while if there was only w, it was perfectly symmetric like that of the Gaussian model. Similar to symmetrical modelling, the heating and the cooling data were separately analysed to optimize the value of equation parameters and find their relationship with the number of cycles (n).

## 2.3 Artificial neural networking model

Artificial neural networking (ANN) is a subset of machine learning (ML) algorithms designed to recognise patterns, learn from data and make predictions. Without prior knowledge of the System, ANN can predict the output based on the valid input in the dataset. ANN is inspired by the biological neural network of the human brain [33, 34]. The structural building blocks of this network are called perceptron. Once the input data is fed into the ANN, it multiplies the data with weights, the optimised values associated with the connection between neurons. The mathematical function of a neural network is given in Eq. 3. Every perceptron solves this equation (Eq. 3) and transfers the data to the next perceptron to solve the same equation but with the optimum weight assigned to that perceptron. The collection of these connected perceptrons is called a neural network.

$$y = g\left(W_o + \sum_{i=1}^n W_i x_i\right) \quad (3)$$

where,  $y$  is the model output,  $W_o$  is the bias,  $W_i$  is the weights corresponding to neurons,  $x_i$  is the input data, and  $g(x)$  is the activation function.

The heating and cooling cycles were separately modelled using ANN in this study for simplicity and better accuracy. The experimental data was divided into training data (80%) and testing data (20%). Mean absolute error was taken as an accuracy parameter. The developed ANN model for heating and cooling cycles had eight hidden layers, with the input variable being temperature and the output variable being heat flow and Linear activation function for the output layer. Relu Activation function was used in the hidden layers to introduce non-linearity to the model. 'rmsprop' optimiser was used because of its better convergence rate.

## 3 Results and discussion

### 3.1 Empirical model

#### 3.1.1 Symmetrical model

The characteristics of all these equation parameters were analysed. For simplification, the heating and cooling curves were separately analysed. It was done to optimise the empirical model by using distinct values of equation parameters for heating and cooling curves. To determine the behaviour of model parameters, such as 'A', 'w' and 'T<sub>c</sub>', during thermal cycling, each of these parameters was individually analysed, as shown in Fig. 2. This analysis mainly focused on the variation in these model parameters with increasing number of cycles ( $n$ ) in terms of a mathematical expression, as shown in Table 1.

Based on the parameters obtained through these expressions, the model was validated with the experimental data for two different cycles chosen arbitrarily, as shown in Fig. 3. Moreover, it was found that adj. R-Square, a measure used in regression analysis to assess the goodness of fit of a model, of the Gaussian curve was found to be 0.9664, i.e. 96.64% was the model's accuracy.

By incorporating the modified equation parameters, as shown in Table 1, the Gaussian equation gives the modified Gaussian model equation (Eq. 4).

$$H_n = H_o + \left( \frac{A_n}{w_n \times \sqrt{\frac{\pi}{2}}} \right) \times e^{-2(T-T_{c(n)})^2/w^2} \quad (4)$$

For validation purposes, the above equation, Eqn, gives the output data. Equation (4) was compared with the experimental output data of thermal cycling experiments obtained from differential scanning calorimetry. The model developed was compared with two different cycles, i.e., the 2nd and the 6th no. of cycles, which were chosen arbitrarily, to confirm the reproducibility of the model developed. As evident, the experimental heat flow varies asymmetrically with

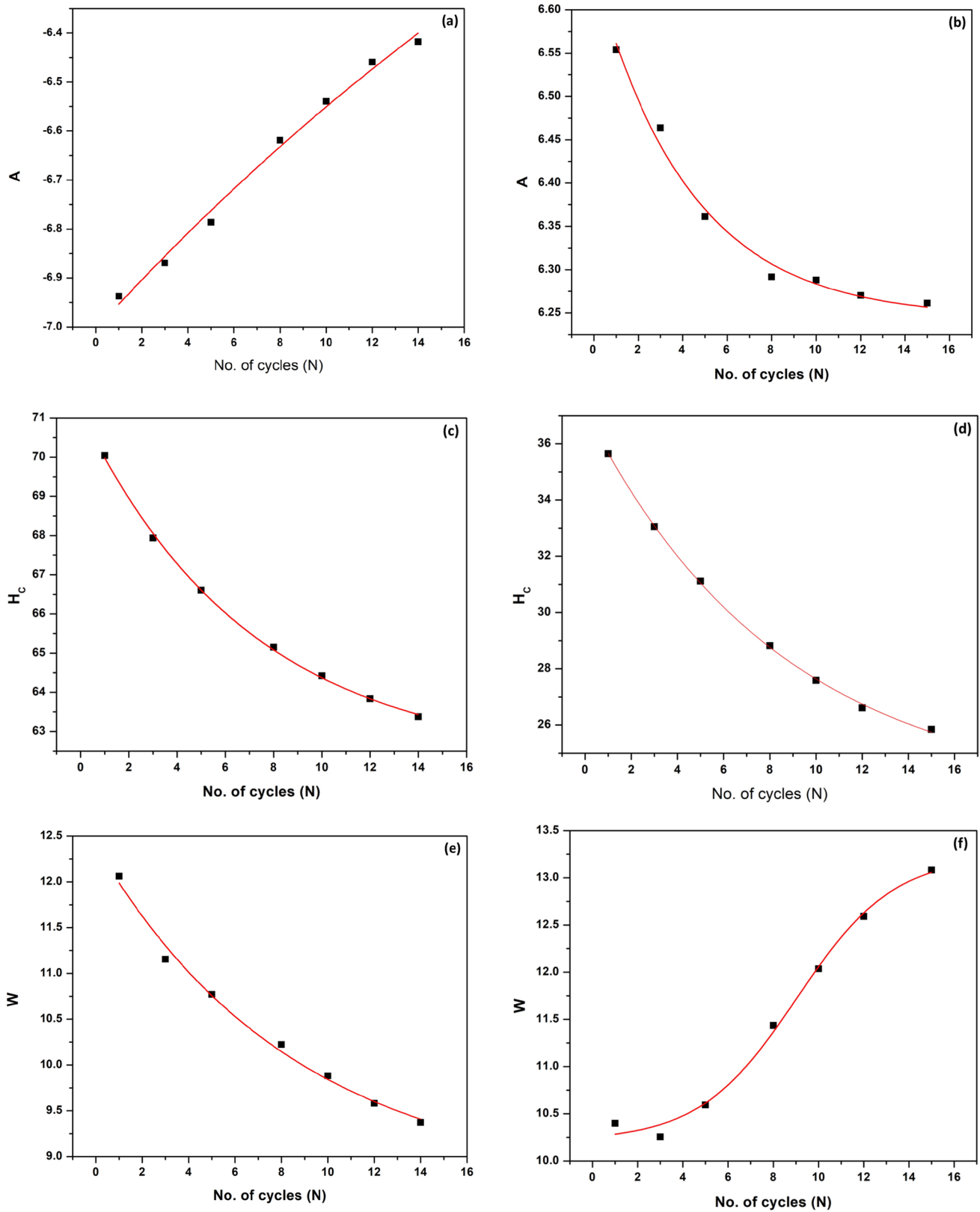


**Fig. 2** Plots showing the variation of symmetrical model parameters, such as A,  $H_c$  and W, during heating (a, c, e) and cooling (b, d, f), respectively

**Table 1** The relationship between the model parameters and the number of cycles(n) for the Gaussian model

Parameters	Expressions
<i>Heating</i>	
$A_{(n)}$	$-5.06 - 1.93 * e^{-0.027 * n}$
$T_{c(n)}$	$62.21 + 8.95 * e^{-0.14 * n}$
$W_{(n)}$	$8.67 + 3.71 e^{0.12 * n}$
<i>Cooling</i>	
$A_{(n)}$	$6.24 + 0.40 e^{-0.23192 * n}$
$T_{c(n)}$	$23.40 + 13.8 e^{-0.12 * x}$
$W_{(n)}$	$13.23 + \frac{(-3.02)}{1 + e^{\frac{n-9.04}{2.15}}}$

temperature, but the Gaussian model is symmetrical about its peak, as shown in Fig. 3. Although the model is not perfect, it can be used to understand the nature of the parameters of the curve.

### 3.1.2 Asymmetrical model

Similar to the Gaussian model, the asymmetrical model was developed and modified by incorporating the number of cycles with each varying model parameter, as shown in Fig. 4. The variations were determined similarly to the Gaussian model, and the expressions correspond to those parameters listed in Table 2. The asymmetrical model has 98.14% accuracy (Adj-R squared = 0.9814), which is better than that for the symmetrical (Gaussian) model. This asymmetrical model can predict the transformation behaviour and the transformation temperatures more precisely than the Gaussian model.

After the relation between the model parameters with respect to the number of cycles is known, the asymmetrical model gives the final equation of the transformation curve, as shown in Eq. (5). The output of this equation (Model output) was now compared with the experimental data. Figure 5 shows that both the experimental and the modelled curves are asymmetrical; hence, this asymmetrical double sigmoidal model closely predicts the heat flow pattern at a given temperature.

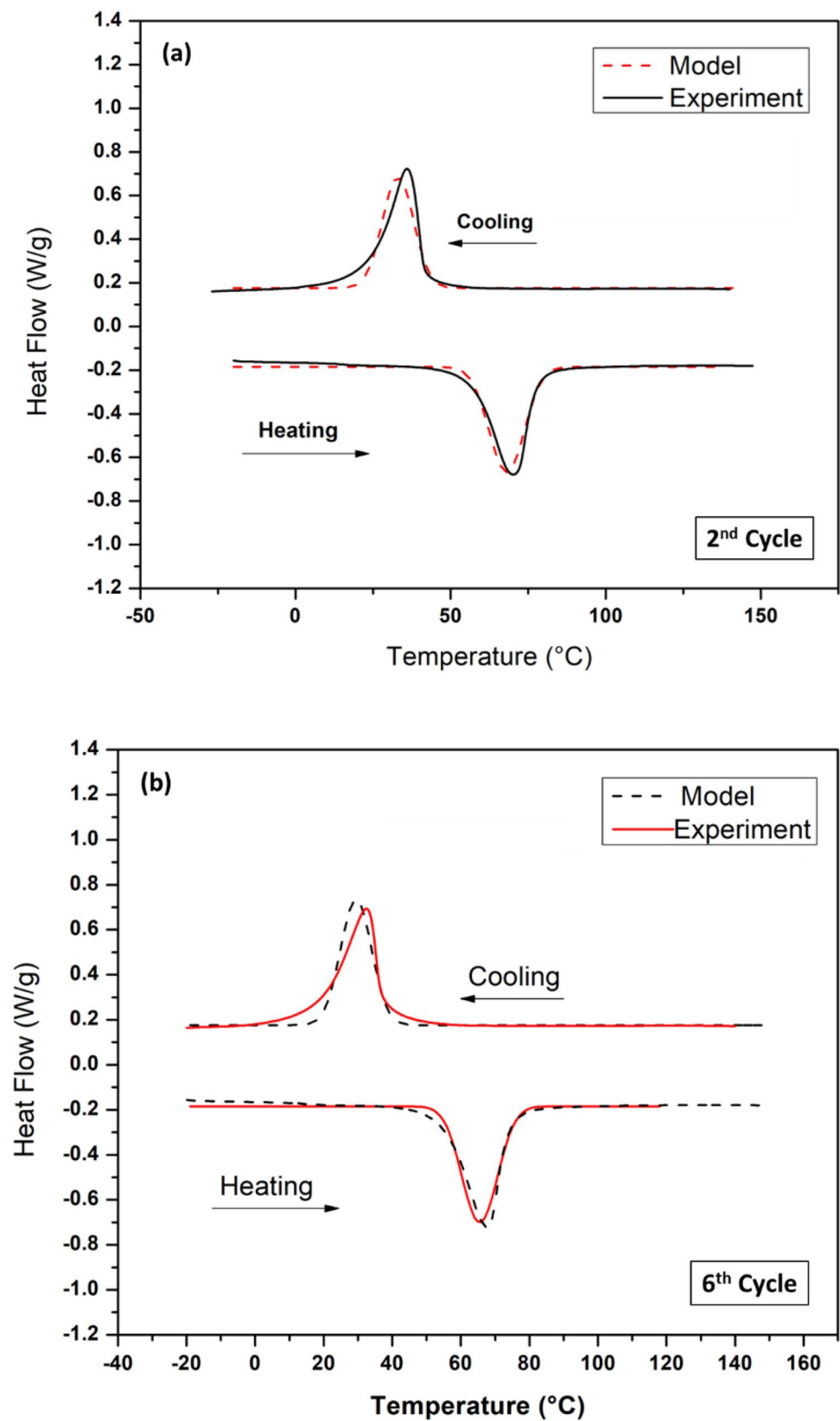
$$H_n = H_o + \left( \frac{A_n}{1 + e^{-\left( \frac{T - T_{c(n)} + \left( \frac{W_1(n)}{2} \right)}{W_2(n)} \right)}} \right) \times \left( 1 - \frac{1}{1 + e^{-\left( \frac{-T - T_{c(n)} - \left( \frac{W_1(n)}{2} \right)}{W_3(n)} \right)}} \right) \quad (5)$$

## 3.2 ANN model

For the cooling cycle, the validation loss of the cooling half was minimised to  $1.43 \times 10^{-6}$ , and the corresponding training loss for that particular epoch was  $6.48 \times 10^{-6}$ . For the heating cycle, the validation loss was minimised to  $1.32 \times 10^{-6}$ , and the corresponding training loss of the same epoch was  $5.3214 \times 10^{-6}$ . The mean absolute error of the heating cycles was minimised to 0.0025, while it was minimised to 0.0012 for cooling. If the mean absolute error is taken as a metric of accuracy for the ANN model, then it comes out to be the average of heating (99.75%) and cooling (99.88%), i.e., 98.14%. The accuracy of prediction is the highest for the ANN model (99.81%) as compared to the symmetrical (96.64%) and asymmetrical (98.14%) models.

From Fig. 6, it can be seen that the ANN model has accurately predicted the transformation behaviour of the NiTi SMA during thermal cycling. Unlike the empirical model, this simple ANN model does not provide the guiding equation but predicts the transformation behaviour directly once the input (no. of cycles and temperature) data is provided. However, the present study is limited by the use of a specific NiTi alloy composition and a controlled experimental setup, which may affect the generalizability of the empirical and ANN models. It also does not account for stress effects or long-term functional fatigue during extensive cycling. Future work can focus on expanding the dataset, exploring alloy compositional variations and stress factors, and studying long-term durability to enhance the applicability of the models.

**Fig. 3** Comparison of Gaussian model with the experimentally obtained DSC thermograms: **a** 2nd cycle and **b** 6th cycle



**Heating cycle parameters ↓**

**Cooling cycle parameters ↓**

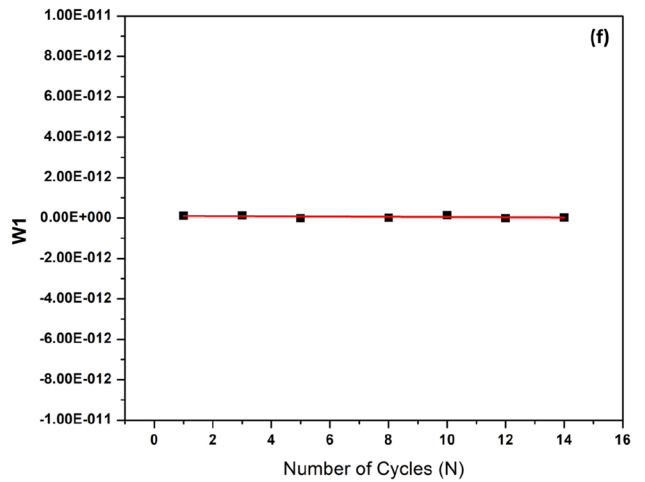
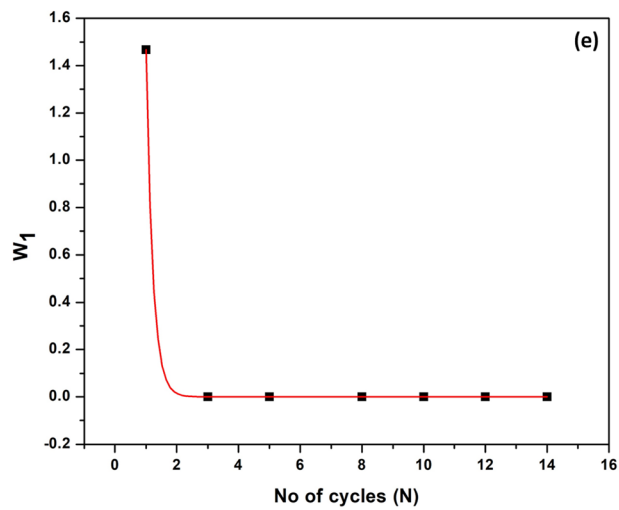
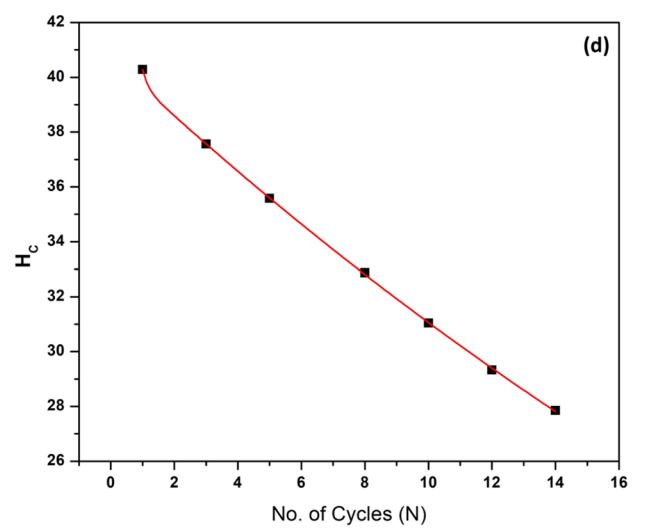
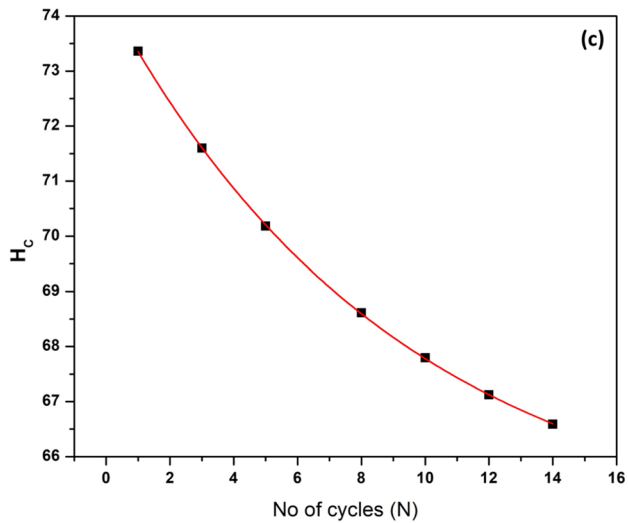
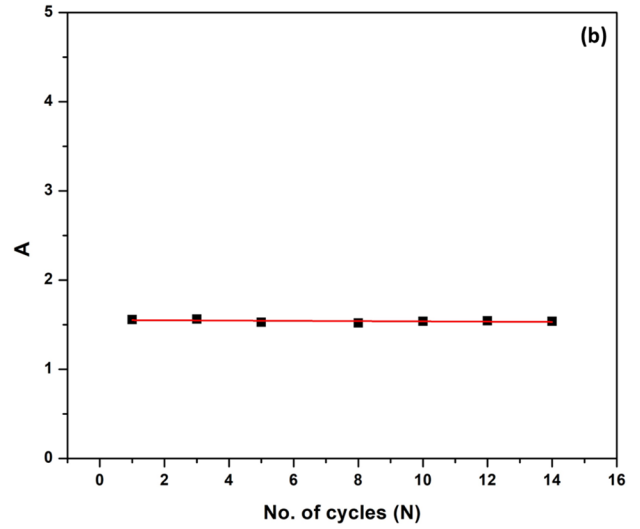
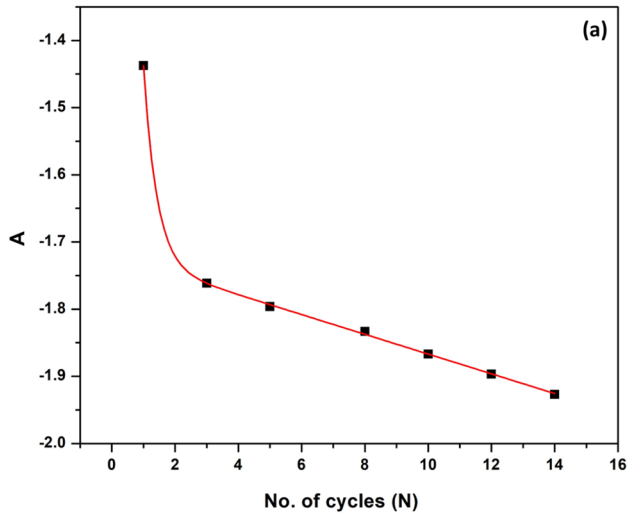


**Fig. 4** Plots showing the variation of asymmetrical model parameters, such as A, H<sub>c</sub> w<sub>1</sub>, w<sub>2</sub> and w<sub>3</sub>, during heating (a, c, e, g, i) and cooling (b, d, f, h, j), respectively

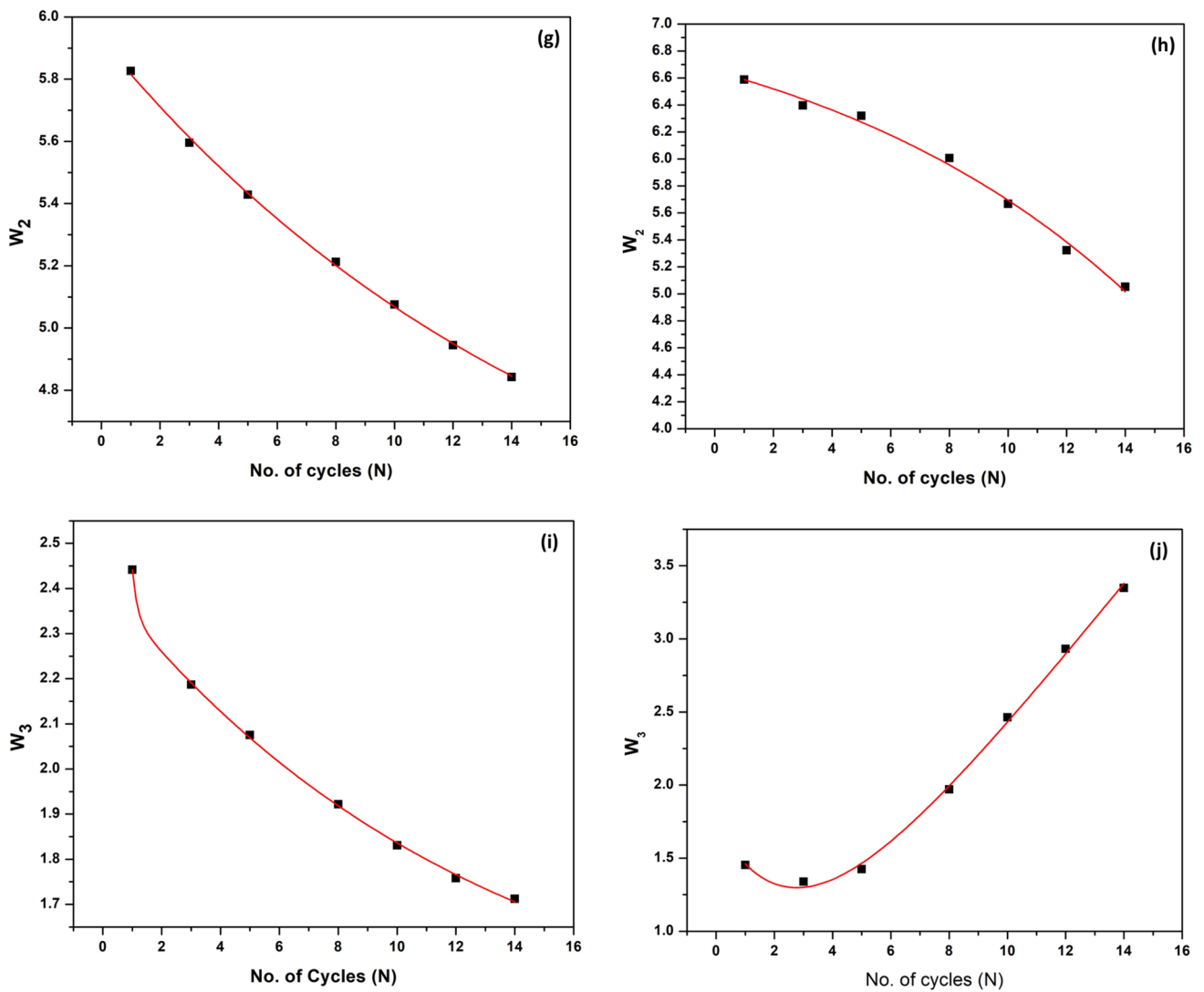
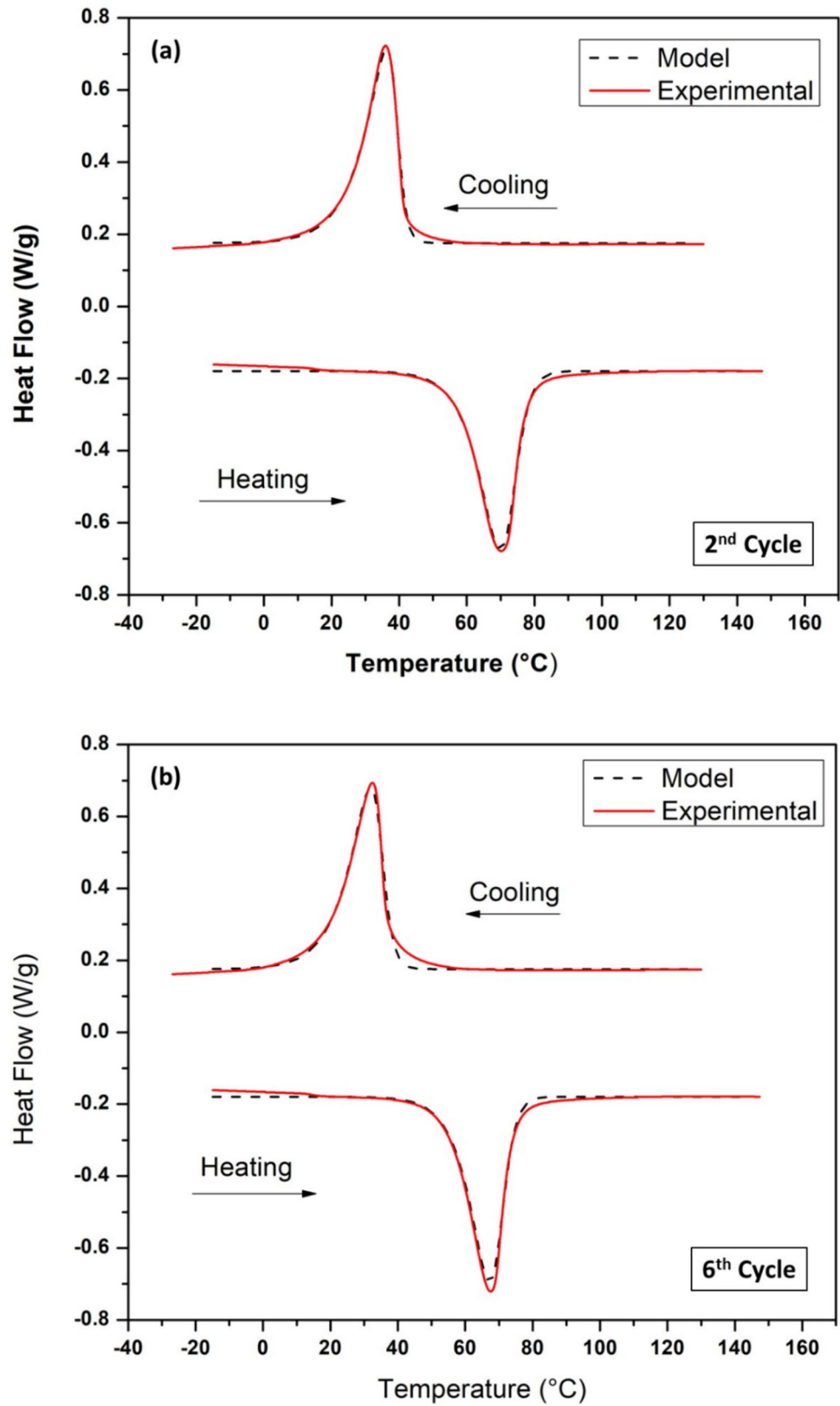


Fig. 4 (continued)

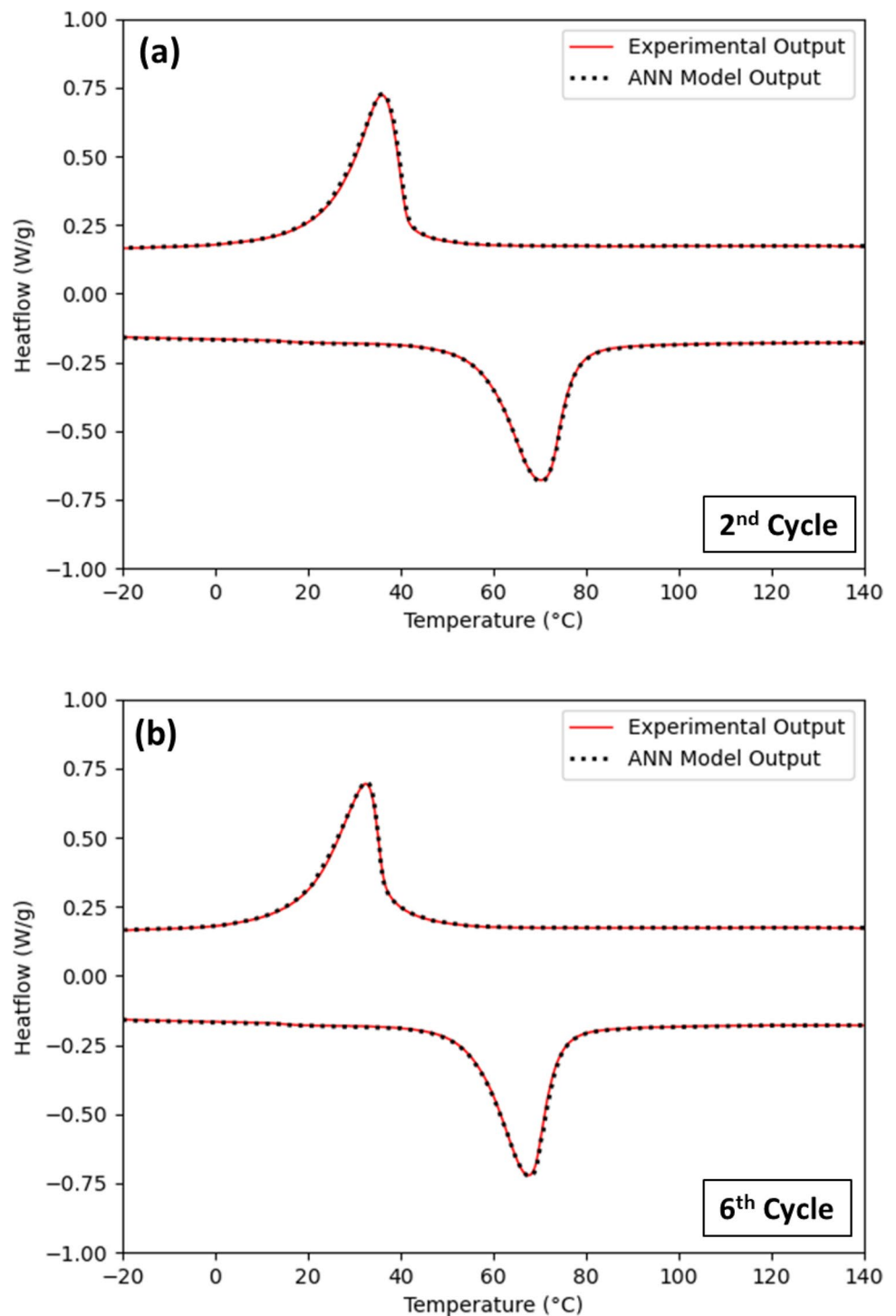
**Table 2** Showing the relationship between model parameters and the number of cycles (n) for the asymmetrical curve model

Parameter	Expression
<i>Heating</i>	
$A_{(n)}$	$(-1.72) + (-0.015)n + (3.16) \cdot (0.09)^n$
$T_{c(n)}$	$64.43 + 9.95 \cdot e^{-0.11n}$
$w_{1(n)}$	$(-1.16E-04) + (1.03E-05)n + (141.18) \cdot (0.01)^n$
$w_{2(n)}$	$4.03 + 1.90 \cdot e^{-0.06n}$
$w_{3(n)}$	$30.40 + (-1.06) \cdot (1 - e^{-\frac{n}{13}}) + (-28) \cdot (1 - e^{-\frac{n}{0.18}})$
<i>Cooling</i>	
$A_{(n)}$	1.54
$T_{c(n)}$	$11.17 + 30.22 \cdot e^{(-0.042 \cdot n)}$
$w_{1(n)}$	6.32E-14
$w_{2(n)}$	$7.364 + (-0.71 \cdot e^{(0.085 \cdot n)})$
$w_{3(n)}$	$(-0.12) + (0.25 \cdot n) + (1.88) \cdot (0.71)^n$

**Fig. 5** Plots show the comparison of experimental data and the asymmetrical model output of (a) the 2nd and (b) the 6th cycles



**Fig. 6** Plots showing the comparison between the ANN Model and the experimental output of **a** 2nd and **b** 6th cycle during thermal cycling



## 4 Conclusion

This study focused on modelling the thermocycling behaviour of a binary NiTi shape memory alloy during thermal cycling. The heat flow at a specific temperature was first found experimentally using a differential scanning calorimeter (DSC), and then the data was analysed for various cycles. Symmetrical, Asymmetrical and ANN models were developed using the same set of experimental data. The symmetrical model was simpler but was not so accurate (96.64%) because of the nature of the experimental output, which is asymmetrical. The asymmetrical model predicts

the behaviour slightly better (98.14%) than the symmetrical model due to the expression's inherent nature to accommodate the transformation's asymmetrical nature. However, the ANN model is highly precise in predicting the transformation behaviour of the NiTi SMA during cycling, with the prediction accuracy being 99.81%.

**Author contributions** S. Ganesan: Conceptualization, Material Resource, Guidance, Experiment Shreyash Pandey: Modelling, Experiment, Draft Writing S. Krishnasamy: Validation of models, Editing and final preparation of the manuscript SMK. Thiagmani: Validation of models, Editing and final preparation of the manuscript.

**Data availability** The raw and processed data to reproduce the results presented in the paper are available in the following repository (controlled access). [https://www.researchgate.net/publication/385875348\\_Raw\\_Data\\_of\\_the\\_work\\_-\\_Prediction\\_of\\_Thermal\\_cycling\\_behaviour\\_of\\_NiTi\\_SMA](https://www.researchgate.net/publication/385875348_Raw_Data_of_the_work_-_Prediction_of_Thermal_cycling_behaviour_of_NiTi_SMA).

## Declarations

**Competing interests** The authors declare no competing interests.

**Open Access** This article is licensed under a Creative Commons Attribution-NonCommercial-NoDerivatives 4.0 International License, which permits any non-commercial use, sharing, distribution and reproduction in any medium or format, as long as you give appropriate credit to the original author(s) and the source, provide a link to the Creative Commons licence, and indicate if you modified the licensed material. You do not have permission under this licence to share adapted material derived from this article or parts of it. The images or other third party material in this article are included in the article's Creative Commons licence, unless indicated otherwise in a credit line to the material. If material is not included in the article's Creative Commons licence and your intended use is not permitted by statutory regulation or exceeds the permitted use, you will need to obtain permission directly from the copyright holder. To view a copy of this licence, visit <http://creativecommons.org/licenses/by-nc-nd/4.0/>.

## References

1. Otsuka K, Ren X. Recent developments in the research of shape memory alloys. *Intermetallics*. 1999;7:511–28. [https://doi.org/10.1016/S0966-9795\(98\)00070-3](https://doi.org/10.1016/S0966-9795(98)00070-3).
2. Hassan AM, Rashid RSM, Ahmad N, Alam S, Hejazi F, Safiee NA. Behaviour of superelastic nickel titanium shape memory alloy material under uniaxial testing and its potential in civil engineering. *MATEC Web Conf*. 2018;203:6005.
3. Lu ZK, Weng GJ. Martensitic transformation and stress-strain relations of shape-memory alloys. *J Mech Phys Solids*. 1997;45:1905–21. [https://doi.org/10.1016/S0022-5096\(97\)00022-7](https://doi.org/10.1016/S0022-5096(97)00022-7).
4. Balci E, Dagdelen F. The comparison of TiNiNbTa and TiNiNbV SMAs in terms of corrosion behavior, microhardness, thermal and structural properties. *J Therm Anal Calorim*. 2022;147:10943–9. <https://doi.org/10.1007/s10973-022-11360-1>.
5. Mohammed SS, Balci E, Dagdelen F, Saydam S. Comparison of thermodynamic parameters and corrosion behaviors of Ti50Ni25Nb25 and Ti50Ni25Ta25 shape memory alloys. *Phys Met Metall*. 2022;123:1427–35. <https://doi.org/10.1134/S0031918X21101130>.
6. Kumar PK, Lagoudas DC. Introduction to shape memory alloys. In: *Shape memory alloys: modeling and engineering applications*. Boston, MA: Springer US; 2008. p. 1–51. [https://doi.org/10.1007/978-0-387-47685-8\\_1](https://doi.org/10.1007/978-0-387-47685-8_1).
7. Hartl DJ, Lagoudas DC. Thermomechanical characterization of shape memory alloy materials. In: *Shape memory alloys: modeling and engineering applications*. Boston, MA: Springer US; 2008. p. 53–119. [https://doi.org/10.1007/978-0-387-47685-8\\_2](https://doi.org/10.1007/978-0-387-47685-8_2).
8. Nemat-Nasser S, Guo W-G. Superelastic and cyclic response of NiTi SMA at various strain rates and temperatures. *Mech Mater*. 2006;38:463–74.
9. Otsuka K, Ren X. Physical metallurgy of Ti-Ni-based shape memory alloys. *Prog Mater Sci*. 2005;50:511–678. <https://doi.org/10.1016/j.pmatsci.2004.10.001>.
10. MohdJani J, Leary M, Subic A, Gibson MA. A review of shape memory alloy research, applications and opportunities. *Mater Design*. 2014;56:1078–113. <https://doi.org/10.1016/j.matdes.2013.11.084>.
11. Velmurugan C, Senthilkumar V, Dinesh S, Arulkirubakaran D. Review on phase transformation behavior of NiTi shape memory alloys. *Mater Today Proc*. 2018;5:14597–606. <https://doi.org/10.1016/j.matpr.2018.03.051>.
12. Xue D, Zhou Y, Ding X, Otsuka K, Sun J, Ren X. Martensite aging effects on the dynamic properties of Au-Cd shape memory alloys: characteristics and modeling. *Acta Mater*. 2011;59:4999–5011. <https://doi.org/10.1016/j.actamat.2011.04.050>.
13. Mihálcz I. Fundamental characteristics and design method for nickel-titanium shape memory alloy. *Periodica Polytech Mech Eng*. 2001;45:75–86.
14. Mwangi JW, Nguyen LT, Bui VD, Berger T, Zeidler H, Schubert A. Nitinol manufacturing and micromachining: a review of processes and their suitability in processing medical-grade nitinol. *J Manuf Process*. 2019;38:355–69. <https://doi.org/10.1016/j.jmapro.2019.01.003>.
15. Olander A. An electrochemical investigation of solid cadmium-gold alloys. *J Am Chem Soc*. 1932;54:3819–33. <https://doi.org/10.1021/ja01349a004>.
16. Buehler WJ, Gilfrich JV, Wiley RC. Effect of low-temperature phase changes on the mechanical properties of alloys near composition TiNi. *J Appl Phys*. 1963;34:1475–7. <https://doi.org/10.1063/1.1729603>.
17. Van Humbeeck J. Non-medical applications of shape memory alloys. *Mater Sci Eng, A*. 1999;273–275:134–48.
18. Melton KN. General applications of SMA's and smart materials. *Shape Memory Mater*. 1998; 220–239.

19. Gao Y, Casalena L, Bowers ML, Noebe RD, Mills MJ, Wang Y. An origin of functional fatigue of shape memory alloys. *Acta Mater.* 2017;126:389–400. <https://doi.org/10.1016/j.actamat.2017.01.001>.
20. Frenzel J. On the importance of structural and functional fatigue in shape memory technology. *Shape Memory Superelastic.* 2020;6:213–22. <https://doi.org/10.1007/s40830-020-00281-3>.
21. Ibarra A, SanJuan J, Bocanegra EH, Nó ML. Evolution of microstructure and thermomechanical properties during superelastic compression cycling in Cu-Al-Ni single crystals. *Acta Mater.* 2007;55:4789–98. <https://doi.org/10.1016/j.actamat.2007.05.012>.
22. Fraj BB, Zghal S, Tourki Z. DSC investigation on entropy and enthalpy changes in Ni-rich NiTi shape memory alloy at various cooling/heating rates. In: Haddar M, Chaari F, Benamara A, Chouchane M, Karra C, Aifaoui N, editors. *Design and modeling of mechanical systems—III: proceedings of the 7th conference on design and modeling of mechanical systems, CMSM'2017, March 27–29, Hammamet, Tunisia.* Cham: Springer International Publishing; 2018. p. 631–9. [https://doi.org/10.1007/978-3-319-66697-6\\_61](https://doi.org/10.1007/978-3-319-66697-6_61).
23. Wang X, Van Humbeeck J, Verlinden B, Kustov S. Thermal cycling induced room temperature aging effect in Ni-rich NiTi shape memory alloy. *Scripta Mater.* 2016;113:206–8. <https://doi.org/10.1016/j.scriptamat.2015.11.007>.
24. Besseghini S, Villa E, Tuissi A. Ni-Ti-Hf shape memory alloy: effect of aging and thermal cycling. *Mater Sci Eng, A.* 1999;273:390–4.
25. Allison J. Integrated computational materials engineering: a perspective on progress and future steps. *JOM.* 2011;63:15.
26. Zaeem MA, Zhang N, Mamivand M. A review of computational modeling techniques in study and design of shape memory ceramics. *Comput Mater Sci.* 2019;160:120–36. <https://doi.org/10.1016/j.commatsci.2018.12.062>.
27. Ganesan S, Vedamanickam S. Transformation behavior of a shape memory Ni<sub>50.7</sub>Ti<sub>49.3</sub> (at.%) alloy during partial thermal cycling. *J Mater Eng Perform.* 2023;32:2501–8. <https://doi.org/10.1007/s11665-022-07284-4>.
28. Deringer VL, Bartók AP, Bernstein N, Wilkins DM, Ceriotti M, Csányi G. Gaussian process regression for materials and molecules. *Chem Rev.* 2021;121:10073–141. <https://doi.org/10.1021/acs.chemrev.1c00022>.
29. Huang X, Jin H. An earthquake casualty prediction model based on modified partial Gaussian curve. *Nat Hazards.* 2018;94:999–1021. <https://doi.org/10.1007/s11069-018-3452-3>.
30. Liu C, Zheng D, Murray A, Liu C. Modeling carotid and radial artery pulse pressure waveforms by curve fitting with Gaussian functions. *Biomed Signal Process Control.* 2013;8:449–54. <https://doi.org/10.1016/j.bspc.2013.01.003>.
31. Ma C, Zhang F, Liu H, Wang H, Hu J. Thermogravimetric pyrolysis kinetics study of tobacco stem via multicomponent kinetic modeling, Asym2sig deconvolution and combined kinetics. *Bioresour Technol.* 2022;360: 127539. <https://doi.org/10.1016/j.biortech.2022.127539>.
32. Chen C, Miao W, Zhou C, Wu H. Thermogravimetric pyrolysis kinetics of bamboo waste via asymmetric double sigmoidal (Asym2sig) function deconvolution. *Bioresour Technol.* 2017;225:48–57. <https://doi.org/10.1016/j.biortech.2016.11.013>.
33. Basheer IA, Hajmeer M. Artificial neural networks: fundamentals, computing, design, and application. *J Microbiol Methods.* 2000;43:3–31. [https://doi.org/10.1016/S0167-7012\(00\)00201-3](https://doi.org/10.1016/S0167-7012(00)00201-3).
34. Soni H, Narendranath S, Ramesh MR. ANN and RSM modeling methods for predicting material removal rate and surface roughness during WEDM of Ti<sub>50</sub>Ni<sub>40</sub>Co<sub>10</sub> shape memory alloy. *AMSE J-AMSE IETA.* 2018;54:435–43.

**Publisher's Note** Springer Nature remains neutral with regard to jurisdictional claims in published maps and institutional affiliations.